a priori value. On the basis of the MSI images of Mathilde, the imaging team determined an average radius of 26.5 ± 1.3 km and a nominal volume estimate of 78,000 km^3 with lower and upper limits of 67,000 km^3 and 90,000 km^3, respectively (*8*). The determined mass and volume estimates for Mathilde then suggest a bulk density estimate of 1.3 ± 0.2 g cm^{-3}.

The bulk density for Mathilde is lower than we expected. However, in the 1989 study of the effects of large numbers of asteroids on the orbit of Mars, Standish and Hellings concluded that the average bulk density for the C-class asteroids was 1.7 ± 0.5 g cm^{-3}. As part of an improved planetary ephemeris development effort, Standish found recently that this average value was 1.2 ± 0.1 g cm^{-3} (*9*). Although Standish noted that the given formal uncertainty on this latter value is undoubtedly optimistic, the result is consistent with the present determination of Mathilde's bulk density. If we assume that Mathilde was formed of black chondritic material (*10*) with a density d of about 2.8 g cm^{-3}, Mathilde's bulk density d_M would be 1.3 g cm^{-3}, suggesting that the asteroid's porosity [$p = 1 - (d_M/d)$] is greater than 50%. This level of porosity would suggest that either Mathilde formed from relatively loosely packed fragments or evolved into a "rubble pile" of material as a result of repeated impacts from other asteroids.

REFERENCES AND NOTES

1. For an overview of the NEAR mission, see *J. Astronaut. Sci.* **43**, 345 (1995). For comprehensive accounts of the Gaspra and Ida encounters by the Galileo spacecraft, see M. J. S. Belton *et al.*, *Science* **257**, 1647 (1992); M. J. S. Belton *et al.*, *Icarus* **120**, 1 (1996).
2. B. G. Williams *et al.*, paper presented at the AAS/AIAA Space Flight Mechanics Meeting, Huntsville, AL, 10 to 12 February 1997.
3. The early Mathilde orbits included only 60 observations over the interval 3 May 1927 to 6 January 1994. In January 1995, E. Goffin made available a data set wherein he had re-reduced many of the existing observations with respect to more modern reference star catalogs and extended the observational interval back to the time of this asteroid's discovery in mid-November 1885. Extensive sets of observations were received from a number of observatories, including McDonald (Texas), Klet (Czech Republic), Modra (Slovakia), Siding Spring (Australia), Oak Ridge (Massachusetts), the Carlsberg Automatic Meridian Circle (Canary Islands), and the U.S. Naval Observatory Flagstaff Station (Arizona). Some of the observations from Flagstaff were reduced with respect to extragalactic radio sources; these observations were given increased weight in the orbit determination process because they were relatively unaffected by the systematic errors present in most reference star catalogs. See R. C. Stone *et al.*, *Astron. J.* **111**, 1721 (1996). Observations taken during the 3 months before the flyby were instrumental in providing an accurate Mathilde ephemeris to the flight project. Beginning on 7 April 1997, observations became available from the observatories of Garradd (Australia), Mauna Kea (Hawaii), and Table Mountain (California). Many of the observations from Table Mountain were reduced with respect to reference stars from the Hipparcos and Tycho star catalogs and were thus upweighted in the orbital solutions because these positions were considered an order of magnitude more accurate than observations reduced with respect to traditional reference star catalogs. Twenty-four of these observations became available covering the dates 21 May, 30 May, 31 May, 17 June, 20 June, 22 June, and 24 June 1997. If these Hipparcos-based positions of Mathilde had not been available before the encounter, and if we had not weighted them strongly in our final orbital solution, the ephemeris errors at encounter would have been at least an order of magnitude larger.
4. Positions for the three bright reference stars in the field were taken from the highly accurate Hipparcos catalog [M. A. C. Perryman, *The Hipparcos Catalogue* (European Space Agency, SP-1200, Noordwijk, Netherlands, 1997)]. Although Hipparcos reference star positions had been made available in advance of publication for improving the orbit of asteroid Ida before the Galileo spacecraft flyby in August 1993 [W. M. Owen Jr. and D. K. Yeomans, *Astron. J.* **107**, 2295 (1994)], the Mathilde encounter marks the first operational use of the Hipparcos catalog by JPL navigation.
5. Our centroiding algorithm modeled the camera's point-spread function as an elliptical Gaussian with 1σ values of 1.7 pixels in the sample direction and 1.0 pixel in the line direction. The DN value in each pixel was modeled by the integrated flux from the point source plus a constant background, with the integration extending over only the light-sensitive part of the pixel. An iterative linearized least-squares procedure then solved for the (x,y) coordinates of the centroid, the brightness of the point source, and the background. This procedure failed at the low signal-to-noise ratio typical of co-added Mathilde images, and we estimated Mathilde's center by eye and lowered the weight appropriately.
6. J. E. Riedel *et al.*, paper presented at the AIAA/AAS Astrodynamics Conference, Portland, OR (20 to 22 August 1990).
7. Besides the spacecraft position and velocity at a 2 June epoch, these parameters include the solved-for magnitude and direction of the maneuver performed on 18 June, nongravitational accelerations, and the Mathilde ephemeris and mass. Error sources treated as considered covariance parameters were the assumed uncertainties in the troposphere and ionosphere refraction and delays, the station location and Earth-moon ephemeris uncertainties, and the optical navigation center-finding and focal length errors. Station range and camera pointing biases were modeled as uncorrelated nondynamic stochastic parameters with a process noise of 0.7 m (range) and 0.01° to 0.03° (camera pointing).
8. J. Veverka *et al.*, *Science* **278**, 2109 (1997).
9. E. M. Standish, personal communication.
10. A. S. Rivkin *et al.*, *Icarus* **127**, 255 (1997).
11. J. Schubart and D. L. Matson, in *Asteroids*, T. Gehrels, Ed. (Univ. of Arizona Press, Tucson, 1979), pp. 84–97.
12. W. Landgraf, *Astron. Astrophys.* **191**, 161 (1988).
13. E. M. Standish and R. W. Hellings, *Icarus* **80**, 326 (1989).
14. E. Goffin, *Astron. Astrophys.* **249**, 563 (1991).
15. G. V. Williams, *Asteroids, Comets, Meteors 1991* (Lunar and Planetary Institute, Houston, TX, 1992), pp. 641–643.
16. B. Viateau and M. Rapaport, *Astron. Astrophys. Suppl. Ser.* **111**, 305 (1995).
17. ———, *Astron. Astrophys.* **320**, 652 (1997).
18. M. J. S. Belton *et al.*, *Nature* **374**, 785 (1995).

19. A portion of this research was carried out by the JPL, California Institute of Technology, under contract to NASA. We thank P. W. Chodas, A. B. Chamberlin, M. S. Keesey, E. M. Standish, and R. N. Wimberly for technical assistance and helpful discussions. Important ground-based astrometric observations of Mathilde were provided by observers including M. Buontempo, D. Clowe, A. Galad, G. J. Garradd, E. Goffin, O. Hainaut, A. K. B. Monet, A. Mrkos, R. McNaught, P. J. Shelus, R. Stone, J. Surace, D. Tholen, J. Ticha, A. Whipple, and R. J. Whiteley. M. J. Perryman of the Hipparcos project kindly provided Hipparcos reference star positions in advance of publication. Prepublication estimates of Mathilde's size and volume were kindly provided by the NEAR MSI team, in particular by P. Thomas and the team chief, J. Veverka. A large part of the success of the very difficult encounter with Mathilde was due to the tireless efforts of the NEAR Flight Team (both at Applied Physics Laboratory and JPL). The outstanding leadership of NEAR's systems engineer, A. Santo, deserves special recognition.

8 October 1997; accepted 12 November 1997

NEAR's Flyby of 253 Mathilde: Images of a C Asteroid

J. Veverka, P. Thomas, A. Harch, B. Clark, J. F. Bell III, B. Carcich, J. Joseph, C. Chapman, W. Merline, M. Robinson, M. Malin, L. A. McFadden, S. Murchie, S. E. Hawkins III, R. Farquhar, N. Izenberg, A. Cheng

On 27 June 1997, the Near Earth Asteroid Rendezvous (NEAR) spacecraft flew within 1212 kilometers of asteroid 253 Mathilde. Mathilde is an irregular, heavily cratered body measuring 66 kilometers by 48 kilometers by 46 kilometers. The asteroid's surface is dark (estimated albedo between 0.035 and 0.050) and similar in color to some CM carbonaceous chondrites. No albedo or color variations were detected. The volume derived from the images and the mass from Doppler tracking of the spacecraft yield a mean density of 1.3 ± 0.2 grams per cubic centimeter, about half that of CM chondrites, indicating a porous interior structure.

The NEAR spacecraft was launched on 17 February 1996 on a 3-year trajectory to the near-Earth asteroid 433 Eros. The spacecraft carries a complement of six science instruments: imager, near-infrared spectrometer, gamma-ray spectrometer, x-ray spectrometer, magnetometer, and laser range finder (*1*); in addition, a radio science investigation analyzes tracking signals from the spacecraft. NEAR will arrive and begin its orbital mission at Eros in early 1999. On its way to Eros, NEAR passed within 1212 km of asteroid 253 Mathilde on 27 June 1997 (2) (Fig. 1).

Discovered in 1885, Mathilde received little attention until it was selected as the target for the NEAR flyby. Observations revealed that Mathilde, an asteroid some 60 km in diameter that orbits the sun at a mean distance of 2.64 astronomical units (AU) (Table 1), is one of the slowest spinning asteroids, taking 17.4 days to complete one rotation (3). Early in the 1970s, remote sensing (4) showed that the bulk of asteroids in the belt could be divided into two broad categories on the basis of albedo and color (and hence composition): the S asteroids, which predominate in the inner part of the belt, and the C asteroids, which are more abundant in the outer half. Spectral reflectance and other remote sensing data identified Mathilde as type C (5). Recent spectral analyses suggest that its surface materials may be similar to those in CI or CM chondrites (6, 7).

The Mathilde encounter took place 1.99 AU from the sun, 4 months after NEAR reached its greatest distance from the sun in its mission. Because the solar panels on NEAR are sized to provide adequate power at the closer heliocentric distances of the Eros orbital phase, there was not enough power to operate all instruments during the flyby. To conserve power and avoid the risk of the spacecraft aborting the flyby sequence if a power shortage developed, only one of the six instruments on NEAR, the multispectral imager (MSI), was turned on for the Mathilde encounter. This imager, an *f*/3.4 refractor with a 244 pixel by 537 pixel charge-coupled device (CCD) camera, has a 2.25° by 2.90° field of view (8).

Six sequences of images were obtained beginning 42 hours before closest approach to perform optical navigation by detecting Mathilde against the star background. Because NEAR was looking toward the sun (solar phase angle of ~140°) as it approached Mathilde, the asteroid was first detected just 36 hours before closest approach as a faint dot almost lost in the sun's glare. By the sixth sequence, 11 hours before encounter, Mathilde had brightened to a visual magnitude of about +7.0 (± 0.3). The spacecraft passed the asteroid at 1212 km, close to the planned 1200-km miss distance (9).

The actual imaging sequence of 534 frames (Fig. 1) began some 5 min before closest approach, when views of a crescent-illuminated Mathilde were obtained at resolutions of about 500 m per pixel. The highest resolution data (160 m per pixel) were obtained at closest approach (1212

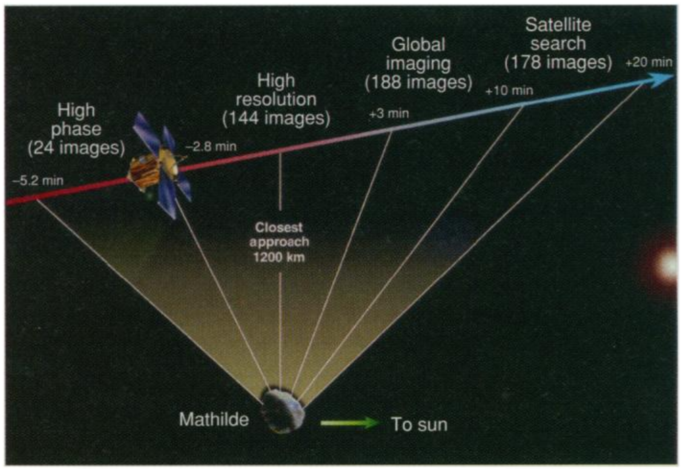

Fig. 1. Schematic time line of the NEAR flyby on 27 June 1997 summarizing the main imaging sequences of 534 frames. The time of closest approach was 12:55:54.5 UT (universal time). The flyby speed was 9.93 km/s.

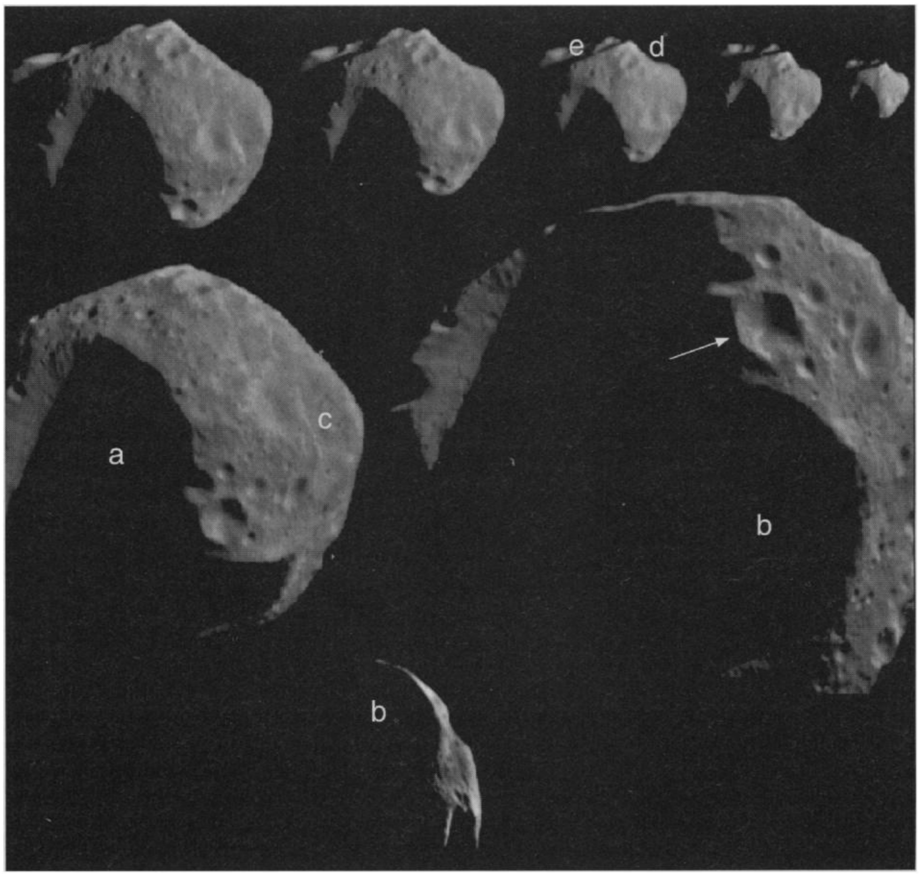

Fig. 2. Representative images of Mathilde. The crescent view obtained before closest approach is at the bottom. The closest approach image (range, 1212 km; resolution, 160 m per pixel) is at lower right; the phase angle was 92°. Proceeding clockwise and shown at a relative scale is the succession of images obtained as NEAR receded from closest approach; these images were obtained over an interval of about 16 min as the range changed from 1780 to 11,540 km (resolution changed from 230 to 1500 m per pixel) and the phase angle varied from 58° to 40°. The five most prominent craters discussed are identified by letters. Crater a has a diameter of 33 km, or slightly more than the asteroid's mean radius. Crater b is estimated to be 26 km across. The 6-km crater indicated by the arrow shows a polygonal outline and collapse or burial of part of its rim (lower right). Crater b also has a polygonal outline, suggesting structural control on crater shape.

J. Veverka, P. Thomas, A. Harch, B. Clark, J. F. Bell III, B. Carcich, J. Joseph, Center for Radiophysics and Space Research, Cornell University, Ithaca, NY 14853, USA.
C. Chapman and W. Merline, Southwest Research Institute, 1050 Walnut Street, Suite 426, Boulder, CO 80302, USA.
M. Robinson, Department of Geological Sciences, Northwestern University, Evanston, IL 60208, USA.
M. Malin, Malin Space Science Systems, Post Office Box 910148, San Diego, CA 92191–0148, USA.
L. A. McFadden, Department of Astronomy, University of Maryland, College Park, MD 20742, USA.
S. Murchie, S. E. Hawkins III, R. Farquhar, N. Izenberg, A. Cheng, Applied Physics Laboratory, Johns Hopkins University, Laurel, MD 20723, USA.

km), when the phase angle was close to 90° (Fig. 2). The imaging sequence continued for another 20 min as the spacecraft receded from the asteroid and viewed Mathilde under good illumination at a phase angle of about 40°. During this time, multicolor global coverage was obtained at 500-m resolution by the MSI's seven color filters, which span the spectral range from 400 to 1100 nm (*8*). The imaging sequence concluded with about 200 images devoted to a satellite search. The MSI is sensitive enough that objects as small as 40 m across could have been detected even if they were made of material as dark as Mathilde (albedo 0.03 to 0.05).

Because of Mathilde's slow rotation, only about half of its surface was seen during the NEAR flyby. Within the 25 min of imaging coverage, no motion of shadows was detected in the images. The expected rotation of Mathilde would produce a motion of only 75 m over 10 min at the equator. The position of Mathilde's pole has not been determined (*3*), and here we have assumed arbitrarily a rotation axis parallel to that of Earth's.

The shape of the visible portion of Mathilde (Table 1) was modeled by stereogrammetry and limb fitting (*10*). Constraints on the unseen portion were provided by observed terminator positions and assumptions about the forms of the largest craters. Mathilde's global shape, which we determined by overlapping large impact craters, is consistent with the observed 0.45-mag amplitude of the light curve (*3*). The nominal triaxial model has diameters of 66, 48, and 46 km, corresponding to a mean radius of 26.5 km, slightly smaller than the 30 km estimated from ground-based observations (*3, 11*). Mathilde's volume is estimated to be 78,000 km^3. A lower limit to the volume, corresponding to a mean radius of 25.2 km, was derived by making the unseen floors of the large craters as deep as seemed physically reasonable (*12*). This minimum-volume model appears unlikely in that it would produce a light-curve amplitude smaller than the 0.45 mag observed (*3*). A maximum-volume model, corresponding to a mean radius of 27.8 km, was obtained by assuming a large bulge in the unseen portion of the asteroid, but one not large enough to make the asteroid so asymmetric as to produce a light-curve amplitude in excess of 0.5 mag (*13*).

Table 1. Mathilde parameters. The orbit parameters are semimajor axis *a*, eccentricity e, and inclination relative to the plane of Earth's orbit *i*.

	Ground-based (3, 5–7, 11)
Orbit	a = 2.6 AU, e = 0.23, i = 6.9°
Type	C
Albedo	0.038
Mean radius	30 km
Light-curve period	17.4 days
Light-curve amplitude	0.45 mag
Probable axes	70 km by 50 km by 50 km
	NEAR
Nominal axes (diameters)	66 km by 48 km by 46 km
Mean radius	26.5 ± 1.3 km
Volume	$78{,}000^{+12{,}000}_{-11{,}000}$ km^3
Mass [from (9)]	(1.033 ± 0.044) × 10^{20} g
Mean density	1.3 ± 0.2 g/cm^3
Surface acceleration	~0.9 cm/s^2
Range of visible topography	~5 km
Preliminary albedo	0.035 to 0.05

Within the ~50% of the total area of Mathilde imaged by NEAR, there are five craters with diameters between 19 and 33 km. The largest and best-imaged crater (crater a in Fig. 2) is 33 km across and may be 5 to 6 km deep. An accurate measurement of the depth is not possible because most of the floor remains hidden in shadow. This crater appears to be the least degraded and probably the youngest of the large craters. For typical impact speeds at Mathilde of about 5 km/s, it would take an asteroid about 1 to 3 km across to excavate a 30-km crater on Mathilde (*14*). Such a crater is expected to produce rim ejecta some 1 km in thickness near the rim if gravity scaling applies (*14*). A second large crater (b), with a diameter of 26 ± 4 km, is partially visible near the terminator and is overlapped by the 33-km structure. A third, much more degraded crater (c) is about 20 km across. Near the southern terminator, a large saddle-shaped region, about 28 to 30 km across (d) is probably an impact scar. There may be one other crater about 25 to 30 km across near the southern limb (e).

All of the significant topographic relief seen in the images is associated with large craters and their rims. The bright limb viewed at closest approach shows relief of 1 km over distances of 3 to 4 km. Slope angles (angle between the normal to the surface and the direction of acceleration due to gravity) on Mathilde reach about 50° for the nominal shape and about 40° for the large-volume model. Slope angles within bowl-shaped craters on other objects are generally under 30°, and angles of repose of loose material are about 30° to 35°, regardless of the magnitude of gravity (*15*). The calculated slopes on Mathilde for the smaller volume model are much larger than those found on other small bodies, such as 951 Gaspra, Phobos, Deimos, Amalthea, Hyperion, and most of 243 Ida (*16, 17*), indicating that the smaller volume model is unlikely.

Small impact craters can be seen on the walls of the largest crater (a in Fig. 2) but at areal densities less than those seen on the intercrater surfaces. This observation, as well as the occurrence of ridges and chutes oriented downslope within this and other large craters, suggests that mass wasting has occurred. The inner walls of the largest crater show definite downslope lineations (top arrow, Fig. 3), and in the bottom of the illuminated area are signs of semicoherent sliding of a surface layer perhaps 200 m thick over a substrate (bottom arrows, Fig. 3). This crater also has a sharp rim crest that, in conjunction with the evidence of downslope movement along the inner walls, points to the possibility that this crater has expanded by collapse of its walls since its formation. In the high-resolution images, craters of varying morphology are seen in the diameter range from 6 km down to the limit of effective resolution of about 500 m,

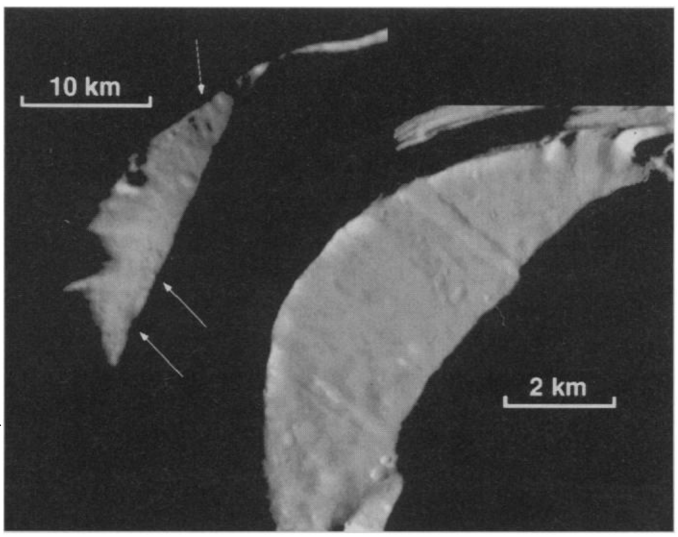

Fig. 3. Comparison of crater rim morphology on Mathilde (top left) and the martian moon Phobos (bottom right). The Mathilde crater in upper left (diameter *D* = 33 km) is viewed at 90° phase; the rim of crater Stickney (*D* = 10 km) on Phobos is viewed at 45° phase. The rim on Mathilde is slightly more cratered. It shows evidence of downslope motion of loose material (arrows) but lacks the grooves seen on the martian satellite.

an observation consistent with the presence of a regolith on Mathilde. Some small craters show evidence of raised rims, but ones that are more rounded and subdued than typical fresh crater rims on the moon (*18*). Craters larger than 5 km show strong polygonality (Fig. 2), indicating structural control, possibly by preexisting fractures. Discrete ejecta blankets are not evident on Mathilde. They are known to be inconspicuous on small bodies and have been detected only in the highest resolution images of Phobos and Ida (*19*). No discrete ejecta blocks have been identified on Mathilde with certainty. Scaling from several small bodies on which ejecta blocks have been detected (*20*) predicts that a 30-km crater on Mathilde should produce blocks up to 200 to 400 m across, which would be only marginally resolvable in our best images.

It is remarkable that Mathilde has withstood a half-dozen severe impacts without betraying more obvious evidence of large-scale fracturing, such as the grooves (Fig. 3) that are associated with the largest crater on Phobos (*21*) and are seen in Galileo images of Gaspra and Ida (*22*). The only possible evidence of a fractured fabric within Mathilde is the occurrence of polygonal-shaped, medium-sized craters.

We assessed Mathilde's cratering history by counting the smaller craters in a 400-km^2 portion of our highest resolution image, in a region of good illumination and modest emission angles. Of the 91 craters identified, 70 exceed our estimated completeness limit of 0.6-km diameter. Mathilde's population of craters with diameters of <3 km is similar in slope and density to Ida's (Fig. 4), which was interpreted to be in saturation equilibrium for craters in this size range (*23*). The similarity of the densities of small craters on Mathilde and Ida suggests similar ages for the surfaces. In the case of Ida, this age has been estimated at 1 to 2 billion years or more (*23*). Crater morphologies on Mathilde range from relatively deep, fresh craters to shallow, degraded ones. Such a range of morphologies is consistent with our inference that Mathilde's surface is in equilibrium with the cratering process.

The number of craters on Mathilde with diameters larger than 5 km exceeds the empirical equilibrium densities seen elsewhere in the solar system (*24*), and the largest craters are near the geometric saturation limit. To first order, the production function of objects that crater asteroids is the same as that responsible for cratering the moon (*25*). In the case of the moon, the production population rises at a positive slope on an R plot for crater diameters larger than about 5 km (*24*, *25*). On a body the size of Mathilde, the observed crater population for large craters should mimic the production function even under saturation. Thus, within our large error bars, the large craters on Mathilde are consistent with a lunarlike cratering production function; the surprise is that Mathilde has retained such large craters and that the craters have not destroyed each other.

Preliminary estimates based on the observed reflectance of Mathilde in the NEAR images place the asteroid's geometric albedo at 0.035 to 0.050, consistent with the nominal value of 0.038 based on telescopic data (*14*). Mathilde's telescopic spectrum is essentially gray (*6*, *7*). Mathilde does not show a feature at a wavelength of 3.0 μm due to water of hydration (*7*). Although an unaltered sample of the hydrated CM meteorite Murchison fails to match Mathilde's spectral properties, a heated sample of Murchison (*26*) provides an excellent match (heating the sample drives off the water of hydration). These findings suggest that no hydrated minerals or aqueous alteration products exist on Mathilde's surface.

Whole-disk NEAR color observations between 400 and 1100 nm agree closely with the telescopic spectral results (*6*, *7*). NEAR found Mathilde to be uniformly bland in both albedo and color (Fig. 5). No significant albedo or color variations are evident in or around the fresher, smaller craters, and none are seen in the interior walls of the 33-km crater that dominates the high-resolution views (*27*). This lack of variation is different from that observed on the S-type asteroids Gaspra and Ida, where material excavated by impacts show small but significant color contrasts with the surroundings (*28*). The lack of color and albedo variations on Mathilde suggests that its interior is made of the same dark, colorless material, as might be expected of a primitive undifferentiated asteroid, and that space weathering has not altered the optical properties of the surface materials (*29*).

The NEAR and ground-based observations (*7*) of Mathilde indicate that its surface lacks hydrated minerals, as would be true of primitive material never heated to the point at which aqueous alteration occurs, or else heated so much that any water of hydration had been driven off. An alternative suggestion (*30*) is that some C-type asteroids are shock-darkened ordinary chondrites. If Mathilde's surface were shock-darkened, one might expect that craters or landslides on crater walls would have exposed non–shock-darkened materials at depth, a prediction inconsistent with the absence of observable color and albedo differences in NEAR images.

The model volumes (Table 1) determined from the MSI images, combined with the mass determination of Yeomans *et al.*

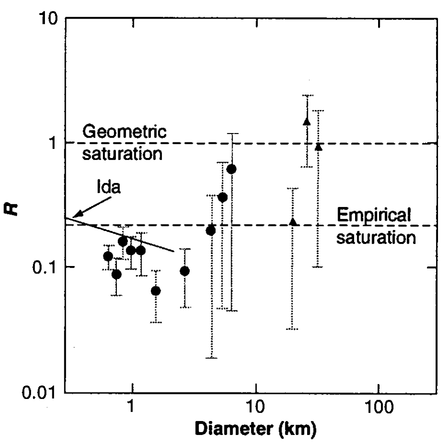

Fig. 4. Spatial density of craters on Mathilde as a function of diameter D. Differential counts are divided by D^{-3} to yield the dimensionless number R (*24*). The R = 1 line represents geometric saturation, the limit to which craters of a given size can be fit onto the surface. On actual surfaces, observed saturation equilibrium yields horizontal lines at a lower level, usually near R = 0.2 (*24*). Triangles are for the large craters discussed in the text; circles indicate smaller craters from a part of the highest resolution image. The observed crater density on Ida (*23*) is shown for comparison.

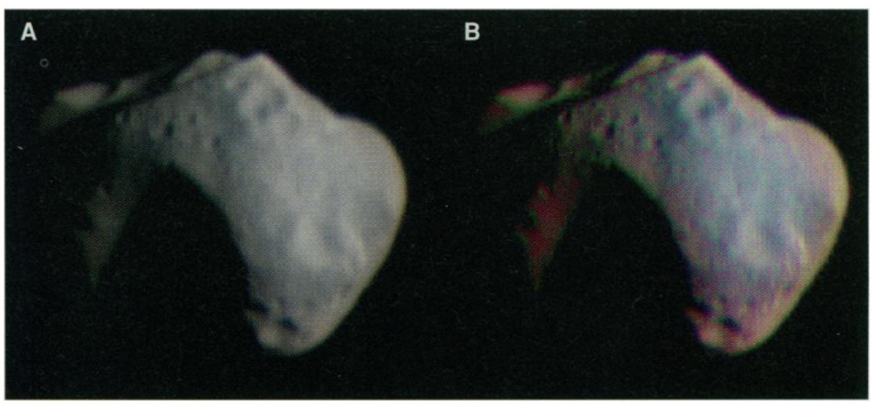

Fig. 5. (**A**) Approximate true color image of Mathilde with brightness enhanced. In (**B**), small visible-color differences have been highly enhanced and overlain on a 550-nm filter image of Mathilde.

(9), yield mean densities of 1.1 to 1.5 g/cm^3. Assuming a nominal value of 1.3 g/cm^3, the density is only half or less that measured for CM meteorites (*31*), indicating a porous, underdense structure for Mathilde's interior. The alternative is that some low-density material such as water ice is preserved within Mathilde's interior, a hypothesis for which there is no supporting evidence and which seems to be at variance with the unhydrated nature of Mathilde's regolith as determined by spectroscopy (*7*). It is possible that Mathilde is a "rubble pile" asteroid, the interior having been pulverized by a long history of collisions (*32*). However, it is also possible that if C-type asteroids are made of primitive, unprocessed materials, then the low density may be primordial. The hydrostatic pressure even at the center of Mathilde is less than 2 bars, insufficient to lithify loose materials. Measured densities for potentially comparable low-albedo, presumably carbonaceous, objects are scarce. Phobos and Deimos have densities of 1.9 and 1.8 g/cm^3, respectively (*33*). The mean density of 1 Ceres (mean radius 460 km) is 2.7 g/cm^3 (*34*).

With the reliable determination of a low density for Mathilde, the probability increases that many asteroids are underdense (have significant internal porosity), as suggested by a variety of cratering and asteroid collisional models (*35–37*). Ida has a mean density of 2.6 ± 0.5 g/cm^3 on the basis of likely assumptions about the orbit of Dactyl (Ida's satellite), a value that implies porosities of 20 to 60% with respect to plausible meteorite analogs (*38*).

Mathilde has a rotation period of 17.4 days; only two asteroids, 288 Glauke and 1220 Crocus, are known to spin more slowly (*39*). Two mechanisms suggested to slow down such objects from the much faster rotation rates (between 5 to 15 hours) observed for most asteroids (*40*) are (i) outgassing of volatiles to remove angular momentum, and (ii) tidal interaction with a large satellite. The first does not seem plausible for Mathilde because no evidence of outgassing is observed. Given the discovery of Dactyl (*41*), the second possibility was considered seriously before the NEAR flyby. Some 200 images were taken between about 10 min (6000 km) and 20 min (12,000 km) after closest approach as the spacecraft receded from the asteroid, covering the sky around Mathilde out to distances of 300 to 600 km (about 10 to 20 radii). We estimate that we imaged some 4 to 5% of the volume of the Hill sphere of stability around Mathilde, calculated to extend to about 100 radii (*42*). The images, generally taken at intervals of 2 s, included a range of exposures up to the maximum of 999 ms possible with the MSI (*8*). Typically, each image (2.25° by 2.90°) contains 2 dozen stars down to the limiting magnitude of +10.5. Cosmic ray noise can be eliminated by comparing successive images. No satellite brighter than 6 to 7 mag, corresponding to an object 200 to 300 m in diameter, was found.

The occurrence of large craters on Mathilde supplements the growing evidence that craters with diameters D comparable to a body's mean radius R_m can form without catastrophically disrupting an object and supports the predictions of several recent hydrocode models of impact processes (*35–37*). Wien Regio, a 15-km-wide depression on Ida, has a D/R_m ratio of 0.95 if the asteroid's R_m is considered, but a ratio ~ 1.5 if the radius of curvature of that end of the elongated asteroid is used (*37*). A 10-km depression on Deimos (R_m = 6.2 km) has a D/R_m ratio of about 1.5 (*17*). Crater Pan on Amalthea has a ratio of 0.95 (*43*). For these objects, the transient crater is nearly as large as the final one; for larger craters on larger objects, comparisons may best be made with estimated transient crater diameters D_t. A 460-km crater on Vesta (R_m = 265 km) suggests a D_t of 290 km and implies D_t/R_m = 1.1 (*44*). The South Pole–Aitken basin on the moon has an estimated D_t/R_m = 0.7 (*45*). Thus, the largest crater on Mathilde is not of unprecedented size relative to the body diameter. The real surprise is that so many large craters can be packed so efficiently on such a small body.

Even more remarkable than the simple existence of these large craters is the degree to which their rim crests and basic shapes seem minimally affected by subsequent large impacts. Although Mathilde has low surface gravity, hydrocode models of impacts predict that a large fraction of crater ejecta will be retained on such an object (*35–37*), a conclusion supported by observations of ejecta deposits on Phobos (*46*) and Ida (*47*). On Mathilde, the large craters do show a range of morphologies, as do the smaller ones, as might be expected from degradational effects due to ejecta. However, the large craters are not erased by the formation of others nearby. One might also expect that seismic shaking associated with large impacts would modify preexisting topography. Evidently this is not the case. One can surmise that Mathilde's composition or internal structure may play some role in localizing the damage from impacts, perhaps by dampening the shock waves generated by the events. This situation is in sharp contrast to asteroids such as Gaspra, where a faceted shape and relative lack of craters has been attributed to major modification of the surface by previous bombardment (*17*).

REFERENCES AND NOTES

1. R. W. Farquhar *et al.*, *J. Astronaut. Sci.* **43**, 353 (1995); S. M. Krimigis and J. Veverka, *ibid.*, p. 345; A. G. Santo *et al.*, *ibid.*, p. 373.
2. A. P. Harch *et al.*, *ibid.*, p. 399.
3. S. Mottola *et al.*, *Planet. Space Sci.* **43**, 1609 (1995).
4. C. R. Chapman *et al.*, *Icarus* **25**, 104 (1975).
5. E. F. Tedesco *et al.*, in *Asteroids II*, R. Binzel *et al.*, Eds. (Univ. of Arizona Press, Tucson, 1989), pp. 290–297.
6. R. P. Binzel *et al.*, *Icarus* **119**, 447 (1996).
7. A. S. Rivkin *et al.*, *ibid.* **127**, 255 (1997).
8. J. Veverka *et al.*, *J. Geophys. Res.* **102**, 23709 (1997).
9. D. K. Yeomans *et al.*, *Science* **278**, 2106 (1997).
10. P. C. Thomas, *Icarus* **105**, 326 (1993); D. P. Simonelli *et al.*, *ibid.* **103**, 49 (1993).
11. E. F. Tedesco *et al.*, in *Asteroids II*, R. Binzel *et al.*, Eds. (Univ. of Arizona Press, Tucson, 1989), pp. 1090–1138; E. Bowell *et al.*, *ibid.*, pp. 524–558.
12. By analogy with craters on other bodies, it was assumed that the depth to diameter ratio did not exceed 0.25.
13. A bulge with a maximum amplitude of 20.5 km can be centered in the unseen hemisphere without violating the light-curve constraint.
14. H. J. Melosh, *Impact Cratering: A Geologic Process* (Oxford Univ. Press, New York, 1989); see also V. C. Ryan and H. J. Melosh, *Eos (Fall Suppl.)* **76**, 336 (1995); S. G. Love and T. J. Ahrens, *Icarus* **124**, 14 (1996); (*36*).
15. A. E. Scheidegger, *Theoretical Geomorphology* (Prentice-Hall, Englewood Cliffs, NJ, 1961).
16. P. C. Thomas *et al.*, *Icarus* **120**, 20 (1996); P. C. Thomas *et al.*, *ibid.* **117**, 128 (1995).
17. P. C. Thomas, *ibid.* **77**, 248 (1989).
18. P. H. Schultz, *Moon Morphology* (Univ. of Texas Press, Austin, 1976).
19. Typically these images have resolutions four times better than the best Mathilde images [P. C. Thomas, *Icarus* **40**, 223 (1979); R. Sullivan *et al.*, *ibid.* **120**, 119 (1996)].
20. S. Lee *et al.*, *ibid.* **68**, 77 (1986); P. Lee *et al.*, *ibid.* **120**, 87 (1996).
21. P. Thomas *et al.*, *J. Geophys. Res.* **84**, 8457 (1979).
22. J. Veverka *et al.*, *Icarus* **107**, 72 (1994); P. Thomas and J. Veverka, *ibid.* **40**, 394 (1979).
23. C. Chapman *et al.*, *ibid.* **120**, 77 (1996).
24. C. Chapman and W. McKinnon, in *Satellites*, J. Burns and M. S. Matthews, Eds. (Univ. of Arizona Press, Tucson, 1986), pp. 492–580.
25. G. Neukum and B. A. Ivanov, in *Hazards Due to Comets and Asteroids*, T. Gehrels, Ed. (Univ. of Arizona Press, Tucson, 1994), pp. 359–416.
26. T. Hiroi, C. M. Pieters, M. E. Zolensky, M. E. Lipschutz, *Science* **261**, 1016 (1993).
27. Spectral variations across Mathilde's surface are small (<5%) and can be attributed to photometric effects. Surfaces tend to appear slightly redder under grazing illumination and viewing. In the NEAR images, regions near the terminator illuminated at large incidence angles appear slightly redder than those illuminated from closer to the normal. On smaller scales, slight color heterogeneities on Mathilde seem to correlate with local slope effects.
28. For Gaspra, see P. Helfenstein *et al.*, *Icarus* **107**, 37 (1994); for Ida, see J. Veverka *et al.*, *ibid.* **120**, 66 (1996).
29. Space weathering may not have a significant effect on surfaces rich in opaque materials [T. V. Johnson and F. P. Fanale, *J. Geophys. Res.* **78**, 8507 (1973)].
30. D. T. Britt and C. M. Pieters, *Proc. Lunar Planet. Sci. Conf.* **20**, 109 (1989); see also C. R. Chapman, *Meteoritics Planet. Sci.* **31**, 699 (1996).
31. Average densities for carbonaceous chondrites are 2.2 to 2.3, 2.6 to 2.9, and 3.3 to 3.6 g/cm^3 for types CI, CM, and CV/CO, respectively [J. T. Wasson, *Meteorites* (Springer-Verlag, New York, 1974)].
32. C. R. Chapman, in *Asteroids: An Exploration Assessment*, D. Morrison and E. C. Wells, Eds. (NASA Conf. Publ. 2053, National Aeronautics and Space Administration, Washington, DC, 1978), pp. 145–160; D. Davis *et al.*, in *Asteroids*, T. Gehrels, Ed. (Univ. of Arizona Press, Tucson, 1979), pp. 528–557.

33. For densities of Phobos, see G. A. Avenesov *et al.*, *Planet. Space Sci.* **39**, 281 (1991); for Deimos, B. G. Williams *et al.*, *Proc. Lunar Planet. Sci. Conf.* **19**, 1274 (1988). Note that D. E. Smith *et al.* [*Geophys. Res. Lett.* **22**, 2171 (1995)] calculated a density of 1.5 g/cm^3 for Phobos.
34. R. Millis *et al.*, *Icarus* **72**, 502 (1987).
35. E. Asphaug and H. J. Melosh, *ibid.* **101**, 144 (1993); S. G. Love and T. J. Ahrens, *ibid.* **124**, 141 (1996).
36. E. Asphaug *et al.*, *ibid.* **120**, 158 (1996).
37. R. Greenberg *et al.*, *ibid.*, p. 106.
38. M. J. S. Belton *et al.*, *Nature* **374**, 785 (1995).
39. A. W. Harris, *Icarus* **107**, 209 (1994); R. P. Binzel, *ibid.* **63**, 99 (1985); A. W. Harris, *Bull. Am. Astron. Soc.* **15**, 828 (1983).
40. R. P. Binzel *et al.*, in *Asteroids II*, P. Binzel *et al.*, Eds. (Univ. of Arizona Press, Tucson, 1989), pp. 416–441.
41. C. R. Chapman *et al.*, *Nature* **374**, 783 (1995); J. Veverka *et al.*, *Icarus* **120**, 200 (1996).
42. P. D. Hamilton and J. A. Burns, *Icarus* **92**, 118 (1991).
43. P. C. Thomas *et al.*, *J. Geophys. Res.* **86**, 8675 (1981).
44. P. C. Thomas *et al.*, *Science* **277**, 1492 (1997).
45. S. Croft, *Icarus* **99**, 402 (1992).
46. P. C. Thomas *et al.*, *ibid.* **107**, 23 (1994).
47. P. Geissler *et al.*, *ibid.* **120**, 140 (1996).
48. This contribution is dedicated to the memory of Jurgen Rahe and Eugene Shoemaker, who played key roles in making the exploration of asteroids a reality. Both were involved in the studies that led to the initiation of the NEAR Project. Rahe, in his role as Science Program Director for Solar System Exploration, oversaw the activities of the project until his tragic death shortly before the Mathilde encounter. Shoemaker participated in the Mathilde encounter activities as a guest of the NEAR Imaging Team. We are grateful to D. Yeomans of NEAR's Radio Science Team for close collaboration in the determination of Mathilde's density, to two reviewers for helpful comments, and to B. Chew, who paid close attention to the preparation of the manuscript. We are especially indebted to the Mission Design, Mission Operations, and Flight teams at the Applied Physics Laboratory, and to the Navigation Team at the Jet Propulsion Laboratory. Special thanks are due to G. Heyler, M. Holdridge, A. Santo, W. Owen, J. Miller, D. Scheeres, B. G. Williams, D. Dunham, D. Morrison, A. Harris, C. Porco, C. Shoemaker, F. Vilas, A. Rivkin, R. Binzel, P. Helfenstein, C. Tector, and M. Roth.

19 September 1997; accepted 19 November 1997

Quantum-Confined Stark Effect in Single CdSe Nanocrystallite Quantum Dots

S. A. Empedocles and M. G. Bawendi*

The quantum-confined Stark effect in single cadmium selenide (CdSe) nanocrystallite quantum dots was studied. The electric field dependence of the single-dot spectrum is characterized by a highly polarizable excited state (~10^5 cubic angstroms, compared to typical molecular values of order 10 to 100 cubic angstroms), in the presence of randomly oriented local electric fields that change over time. These local fields result in spontaneous spectral diffusion and contribute to ensemble inhomogeneous broadening. Stark shifts of the lowest excited state more than two orders of magnitude larger than the linewidth were observed, suggesting the potential use of these dots in electro-optic modulation devices.

Optical switches are a key component in many optical computing and fiber-optic communication designs. In particular, devices based on the quantum-confined Stark effect (QCSE) in quantum wells (QWs) have proven useful in many optical modulation applications (*1*). In these devices, quantum confinement in one dimension allows the formation of excitonic states with electric field induced Stark shifts many times greater than the electron-hole binding energy (*1*). As a result, the Stark effect in QWs is significantly enhanced relative to that in bulk materials. Quantum dots (QDs), the zero-dimensional analog of QWs, represent the ultimate in semiconductor-based quantum-confined systems (*2*). Narrow transition linewidths inherent in QDs (*3–5*), coupled with large Stark shifts, should result in electro-optic modulation devices with even greater efficiency.

Nanocrystallite QDs synthesized as colloids are a particularly flexible material for such QD heterostructures. In particular, CdSe nanocrystallite QDs, with a band gap tunable throughout the visible range, have been extensively studied as a prototypical QD system. These dots can be synthesized in macroscopic quantities with diameters that are tunable during synthesis (*6*). They are easily incorporated into a variety of insulating and conducting polymers as well as thin films of bulk semiconductors (*7*). They can also be manipulated into close-packed glassy thin films (*8*) and ordered three-dimensional arrays (*9*).

In addition to possible device applications, the QCSE can be used to probe the nature of the excited states in QDs. Delocalized exciton states within the QD core should be highly polarizable, whereas localized surface trap states should have a strong dipole character. Spectral broadening, due to structural and environmental inhomogeneities, has generally complicated the interpretation of ensemble optical studies, including Stark measurements. For example, although the presence of an excited-state dipole has been suggested in ensemble Stark absorption studies (*10*), nearly identical Stark data have also been interpreted without the need for a polar state (*11*).

The elimination of inhomogeneous broadening through single QD spectroscopy has allowed many fundamental observations in recent years (*3–5*, *12–14*). In this report, we use fluorescence microscopy to study the QCSE in single CdSe nanocrystallite QDs of varying sizes.

Five sample sizes were studied. The QDs were synthesized as in (*6*), with average radii of 22, 24, 26, 29, and 37.5 Å. The 37.5 Å sample was further divided, and half of the sample was overcoated with a ~6 Å layer of ZnS (*15*). The 24 Å sample was also overcoated with ZnS. We applied electric fields by using photolithographically patterned Ti-Au electrodes on a crystalline quartz substrate. The electrodes were patterned in an interdigitated design with an interelectrode spacing of 5 μm and a height of 1200 Å. A dilute solution of QDs in hexane was placed over the electrodes and was immediately wicked from the surface, leaving only a small number of dots adsorbed to the substrate. Spectra were taken from dots located midway between adjacent electrodes to ensure a uniform electric field (*16*). We took single dot spectra at 10 K using a far-field epifluorescence microscope [described elsewhere (*3*)] with 514-nm excitation from an Ar^+ laser.

In a series of emission spectra taken from the same single dot with the applied electric field either on or off (Fig. 1A), a single peak corresponding to the zero phonon line (ZPL) can be observed shifting between two distinct energies in response to the field. This shift is highly reproducible and results in a change in energy that is 15 times greater than the observed, resolution-limited linewidth and more than two orders of magnitude greater than the linewidths previously reported for the emitting state (*3*). Although the first absorbing state has not yet been characterized for single CdSe QDs, even conservative estimates based on ensemble measurements suggest that this shift is approximately an order of magnitude greater than the width of this state (*17*).

Under a range of electric fields, the peak shifts continuously over more than 60 meV (Fig. 1B). The slight change in zero-field energy over the series is due to spontaneous spectral diffusion (*3*, *12*, *13*). Shifts as large as 75 meV were observed in dots from this sample. These shifts are comparable to room-

Department of Chemistry, Massachusetts Institute of Technology, Cambridge, MA 02139.

*To whom correspondence should be addressed.